# NUMERICAL MODELING OF BUONGIORNO'S NANOFLUID ON FREE CONVECTION: THERMOPHORESIS AND BROWNIAN EFFECTS

**Shatay Khatun[1] and R. Nasrin[2,*]**

[1]Department of Mathematics, European University of Bangladesh, Dhaka-1216, Bangladesh.
 Email: shataykhatun@eub.edu.bd
[2]Department of Mathematics, Bangladesh University of Engineering & Technology, Dhaka-1000, Bangladesh.
*Email: rehena@math.buet.ac.bd

**Abstract:**

*In this research, numerical modeling is conducted on free convective flow inside a trapezoidal domain with sinusoidal material and temperature allocations at both inclined boundaries using Buongiorno's nanofluid. The model considers thermophoresis with Brownian activity effects taking place in the flow, temperature as well as concentration contours. Non-uniform nanoparticle solid concentration and temperature allocations have been imposed at both inclined surfaces. Top and bottom parallel surfaces have been kept as adiabatic. All the walls have been considered as no-slip and impermeable. The leading equations in addition border conditions are initially converted into a dimensionless pattern by a suitable similarity transformation and then resolved arithmetically employing the finite element technique with Galerkin's residual. Buongiorno's model of nanofluid on thermal and material transports, and flow structure has been investigated in detail. Outcomes have been displayed in the form of velocity, temperature, and concentration contours with various governing factors like Brownian action, Lewis number, Buoyancy relation, thermophoresis, Rayleigh number, Prandtl number, etc. Also, the rate of thermal transport has been calculated. The thermophoresis and Brownian effects on velocity, heat, and material fields are identified and finally, the flow, heat, and concentration controlling parameters for a specific material and thermal transport applications inside a trapezium-shaped cavity are obtained. Result demonstrates that the increase of Brownian action guides to enhance thermal transport by 34.75 and 34.27% for the right and left walls, respectively.*

*Keywords:* Buongiorno's nanofluid model; Brownian motion; thermophoresis; free convection; sinusoidal temperature and concentration.

## NOMENCLATURE:

| | | | |
|---|---|---|---|
| $C_p$ | Concentration $(mol.m^{-3})$ | $T$ | Temperature $(K)$ |
| $C$ | Specific heat $(Jkg^{-1}K^{-1})$ | $u, v$ | Velocity along co-ordinates $(ms^{-1})$ |
| $D$ | Coefficient due to diffusivity $(m^2s^{-1})$ | $U, V$ | Non-dimensional velocities |
| $G$ | Force due to gravity force $(ms^{-2})$ | $x, y$ | Cartesian co-ordinates $(m)$ |
| $h$ | Local convective heat transfer coefficient $(Wm^{-2}K^{-1})$ | $X, Y$ | Dimensionless co-ordinates |
| | | **Greek Symbols** | |
| $H$ | Reference height $(m)$ | $\beta$ | Thermal expansion coefficient $(1/K)$ |
| $K$ | Thermal conductivity $(Wm^{-1}K^{-1})$ | $\rho$ | Density $(kgm^{-3})$ |
| $Le$ | Lewis Number | $\theta$ | Dimensionless temperature |
| $n$ | Dimensional perpendicular distance $(m)$ | $\mu$ | Dynamical viscosity $(Nsm^{-2})$ |
| $N$ | Non-dimensional distance | $\alpha$ | Thermal diffusivity $(m^2/s)$ |
| $Nb$ | Brownian action | $\varphi$ | Dimensionless concentration |
| $Nr$ | Buoyancy ratio | $\varepsilon$ | Dimensionless amplitude |
| $Nt$ | Thermophoresis | **Subscript** | |
| $Nu$ | Mean Nusselt number | $c$ | Cold |
| $P$ | Pressure $(kgms^{-2})$ | $h$ | Hot |
| $Pr$ | Prandtl number | $f$ | Fluid |
| $Ra$ | Rayleigh number | | |

---

## 1. Introduction

Buongiorno's model is employed to explore Brownian motion and thermophoresis on flow, heat, and mass transfer. One of the efficient slothful approaches is using nanofluid in heat transport advancement for enhancing the proficiency of thermal systems like thermal storage, photovoltaic/thermal design, heat exchangers, biomedical devices, solar collectors, nuclear reactors, cooling of electronic components, etc. To optimize the heat transfer of nanomaterial using Buongiorno's model is a valuable tool. With this model, thermophysical properties of nanofluid can be derived. These thermophysical properties give the ability of the thermal performance of many electronic devices. So, this model is a handy tool in many engineering sectors. Buongiorno's nanofluid model is appropriately utilized in the study of fluid flow and heat transfer in the microchannel.

Elshehabey and Ahmed (2015) sought MHD mixed convection in a lid-driven cavity loaded by nanofluid applying sinusoidal temperature distribution using Buongiorno's nanofluid model. The legitimacy of Brownian motion and thermophoresis are also incorporated into the nanofluids. The attained result exhibits that an inclined magnetic field in the flow region leads to losing the fluid movement. The fluid was subjected to the exercise of the upper wall for the highest value of the buoyancy ratio. Sheikholeslami et al. (2014) analyzed natural convection taking into account the effect of Brownian motion and thermophoresis. Their result alluded that the Nusselt number decreases Hartmann number and Lewis number, whereas an increasing function of buoyancy ratio number. Suriyakumar and Devi (2019) performed magneto-nanofluid flow, including the exorcism of Brownian motion and thermophoresis. The authors are concerned with the numerical investigation of steady mixed convective magneto nanofluid flow due to an inclined stretching surface under the effects of Brownian and thermophoresis diffusion. Falana et al. (2016) studied the Brownian movement and thermophoresis effects on a stretching sheet numerically. Revnic et al. (2019) showed the dominance of border temperature variations on free convection inside a trapezium Buongiornos' model. They observed that the Nusselt number is an increasing function of the Rayleigh number and wave number.

Esfandiary et al. (2016) conducted natural convective heat alteration considering Brownian motion and thermophoresis effects. The authors demonstrated that the slip velocity mechanisms had caused the decreasing Nusselt number with increasing volume fraction of nanoparticles. They also indicated essential differences between single-phase and two-phase models. Zargartalebi et al. (2016) studied the natural convection in an enclosure within inclined local thermal non-equilibrium porous fin considering Buongiorno's model. The authors tried to show the different behavior of heat transfer for different values of fin angles and lengths. Alam et al. (2015) studied the effect of thermophoresis and Brownian motion on the unsteady forced convective flow of a nanofluid along with a porous wedge with variable suction.. Behbahan and Pop (2015) studied the Brownian motion and thermophoresis effects on the natural convection of nanofluids in a square enclosure with two pairs of heat source/sink. Their study showed an improvement in heat transfer rate for the whole range of Rayleigh numbers by considering Brownian motion and thermophoresis effects.

Sheremet et al. (2014) discussed the free convection in a shallow and slender, porous cavity filled by nanofluids using Buongiorno's model numerically. They focused on Lewis number, the buoyancy ratio, aspect ratio, Rayleigh number, and fluid flow and heat transfer. Elshehabey and Ahmed (2015) numerically investigated MHD mixed convection in a lid-driven pit filled a nanofluid with sinusoidal temperature distribution on the vertical walls using Buongiorno's nanofluid model. Haddad et al. (2012) studied the natural convection in nanofluids due to thermophoresis and Brownian motion in heat transfer enhancement. Matin and Ghanbari (2014) studied the effect of Brownian activity and thermophoresis on the mixed convection of nanofluid in a porous channel, including flow reversal. Aminfar and Haghgoo (2012) investigated the effects of Brownian motion and thermophoresis on natural convection heat transfer of alumina-water nanofluid. They concluded that using a single-phase homogeneous method does not seem reasonable for modeling this class of natural convection. Alsabery et al. (2017) discussed spatial sidewall temperature variations on transient natural convection of a nanofluid in a trapezoidal cavity. The main object of this paper was to examine the effects of non-uniform border temperature variations on time-dependent free nanofluid convection within a trapezium: Buongiorno's nanofluid model. Sheremet and pop (2014) studied natural convection in a square porous cavity with sinusoidal temperature distributions on both side walls filled with a nanofluid using Buongiorno's model. They applied the symmetric sinusoidal temperature concerning the mid-plane of the enclosure. Sivasankaran and Bhuvaneswari (2013) studied natural convection in a porous cavity with sinusoidal heating on both sidewalls. Oriented magneto-conjugate heat transfer and entropy generation investigated by Priam and Nasrin (2021). The authors found 11.62 and 56.72% reduced rate of thermo-fluid energy transfer for the highest magnetic field strength and increase of cavity tilting, respectively. Malvandi et al. (2016) analyzed thermophoresis and Brownian motion effect on heat transfer

enhancement at film boiling of nanofluids. Garoosi et al. (2015) investigated Numerical simulation of natural convection of the nanofluid using a Buongiorno's model. Garoosi et al. (2014) studied numerical simulation of natural convection and mixed convection of the nanofluid in a square cavity using Buongiorno model. Sayyar and Saghafian (2017) simulated the convective heat transfer of nonhomogeneous nanofluid numerically using Buongiorno's model. Malvandi and Ganji (2014) studied Brownian motion and thermophoresis effects on slip flow of Alumina water nanofluid inside a circular microchannel in the presence of a magnetic.

Kata et al. (2019) discussed the impact of thermophoresis and Brownian motion on the melting heat transfer of a Jeffrey fluid near a stagnation point towards a stretching surface using Buongiorno's model. Qasim et al. (2016) studied heat and mass transfer in a nanofluid thin film over an unsteady stretching sheet using Buongiorno's model. Pop et al. (2016) studied the free convection in a non-equilibrium porous cavity considering Buongiorno's model. Noghrehabadi et al. (2013) studied nanofluid's natural convection over vertical plate embedded in the porous medium. Sayyar and Saghafian analyzed (2017) numerical simulation of convective heat transfer of non-homogeneous nanofluid using Buongiorno model. Ali et al. (2021) analyzed boundary layer nanofluid flow over a stretching porous wedge-shaped surface. The authors converted the governing PDEs into ODEs and solved them by QLM with MATLAB bvp4c. Soleimani et al. (2012) studied natural convection heat transfer within a copper-water nanofluid filled a semi-annulus cavity. Their results showed an optimum turn angle for which the heat transfer rate is the maximum for several thermal Rayleigh numbers. Sheremet et al. (2015) discussed steady-state free convection in a right-angle porous trapezoidal cavity filled by a nanofluid: Buongiorno's mathematical model. Garoosi et al. (2015) used the Buongiorno model to oversee the simulation of the nanofluid's natural convection numerically. Al-Weheibi et al. (2017) explore the natural convection heat transfer numerically in a trapezoidal enclosure filled with nanoparticles. Esfe et al. (2016) studied natural convection in a trapezoidal section filled with carbon nanotube and water-ethylene glycol. Ramachandra and Suryanarayana (2018) studied heat and mass transfer of Buongiorno's model nanofluid over a linear and nonlinear stretching surface with thermal radiation and chemical reaction.

Khan et al. (2017) analyzed a numerical study of nanofluid flow and heat transfer over a rotating disk using Buongiorno's model. Demirdzic et al. (1992) studied the fluid flow and heat transfer for non-orthogonal grids: Benchmark. De Davis et al. (1983) looked at the natural convection in a square cavity: Venkatadri et al. (2019) simulated the natural convection heat transfer in a two-dimensional trapezoidal enclosure and found that the fluid flow within the chamber formed with different shapes for different values of Prandtl number. The flow rate was increased by enhancing the Rayleigh number. Ali et al. (2017) found the similarity solution of unsteady MHD boundary layer flow and heat transfer past a moving wedge in a nanofluid using the Buongiorno model. Nasrin et al. (2013) discussed the effect of heating wall position on forced convection along with two-sided open enclosure with porous medium utilizing nanofluid. Ishrat Zahan et al. (2018) studied MHD effect on conjugate heat transfer in a nanofluid filled rectangular enclosure. Nasrin et al. (2020) analyzed the performance of hybrid nanofluid on the enhancement of fluid thermal conductivity in lid-driven undulated cavities. Taylor and Hood (1973) find a numerical solution of Navier-Stokes's equations using finite element technique. Nasrin et al. (2021) found turbulent nanofluid flow passing a shell and tube thermal exchanger with Kays-Crawford model.

The above literature review served that few types of research have been done using Buongiorno's model (2006). Despite these researches, more investigations are still needed, especially Brownian motion and thermophoresis on flow, temperature and concentration fields due to their vast applications. Buongiorno's model can consider the impact of nanoparticle volume fraction distribution. This model can also analyze the heat transfer phenomena due to Brownian motion and thermophoresis using transformations. In addition to the physical design of the present model, selection, fluid flow, and heat transfer are observed, which can significantly influence thermal performance, especially in the field of heating and cooling electronic components. The governing equations transform into ordinary differential equations that are easy to solve more accurately. Thus, the numerical study of Brownian movement and thermophoresis on free convective water-based nanofluid flow in a trapezoidal enclosure using Buongiorno's model will conduct in this research. The research output may apply in heat transfer and flow in solar ponds and air conditioning in the room. The fluid flow and heat transfer of Buongiorno's model give the velocity profile of the nanoparticles and temperature profile numerically. The heat transfer may be convective or non-convective and characterized by various parameters.

## 2. Physical Modeling

Figure 1 expresses the corporeal representation of the considered geometry. This representation has a 2D trapezoidal enclosure of height 1.3 m. The length of top, bottom, and inclined walls is 1, 1.8 and 1.36 m,

respectively. Top and bottom parallel surfaces have been kept as adiabatic. All the walls have been considered no-slip and impermeable. The heat and material allocations of sinusoidal pattern have been compelled in both vertical inclined boundaries. An insulation criterion is set for thermal and material allocations at both bottom and top boundaries. Here, the inclination angle is 17.5 degree. The inclined boundaries make this angle with vertical lines according to clockwise and anticlockwise directions, respectively. The gravitational force is acting vertically downward. No viscous dissipation and chemical reaction are considered but there is Brownian action as well as thermophoresis effects. The nanoparticle and water are thermally at the equilibrium position. Boungiorno's estimation was issued for determining the density difference at the buoyancy expression where nanofluid's other thermo-physical criteria are considered fixed.



Sinusoidal temperature and concentration

Figure 1: Physical model

Sinusoidal temperature and concentration
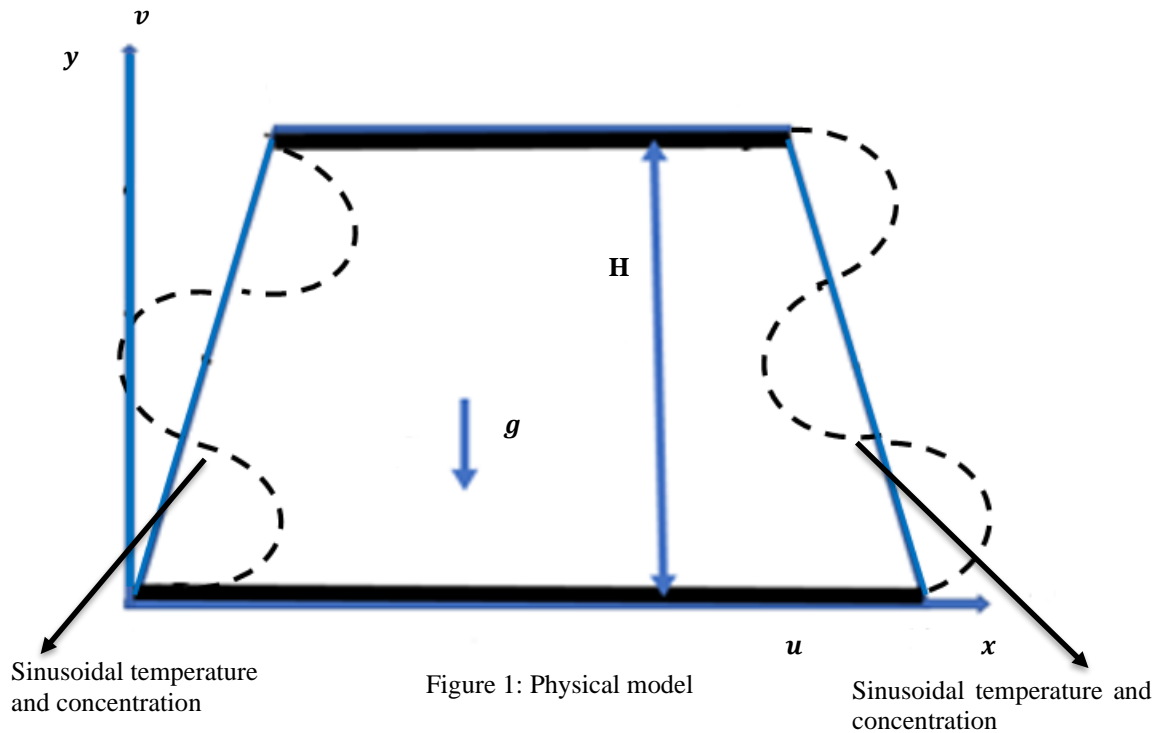
### 3. Mathematical Modeling

The fluid domain inside the cavity has been considered as a continuum. The flow is assumed to be incompressible and insignificant thermal radiation, external force, chemical reaction, and viscous dissipation. The leading PDEs of the fluid in terms of mass, momentum, energy and material conservation equations in the dimensional form have been given bellow:

**Continuity equation**

$$\left(\frac{\partial u}{\partial x} + \frac{\partial v}{\partial y}\right) = 0 \tag{1}$$

**X-momentum equation:**

$$\rho_f \left(u\frac{\partial u}{\partial x} + v\frac{\partial u}{\partial y}\right) = -\frac{\partial P}{\partial x} + \mu_f \left(\frac{\partial^2 u}{\partial x^2} + \frac{\partial^2 u}{\partial y^2}\right) \tag{2}$$

**Y-momentum equation:**

$$\rho_f \left(u\frac{\partial v}{\partial x} + v\frac{\partial v}{\partial y}\right) = -\frac{\partial P}{\partial y} + \mu_f \left(\frac{\partial^2 v}{\partial x^2} + \frac{\partial^2 v}{\partial y^2}\right) + \{C\rho_p + (1-C)[(\rho_f(1-\beta(T-T_c))]\}g \tag{3}$$

**Energy conservation equation:**

$$u\frac{\partial T}{\partial x} + v\frac{\partial T}{\partial y} = \alpha_f \left(\frac{\partial^2 T}{\partial x^2} + \frac{\partial^2 T}{\partial y^2}\right) + D_B \left(\frac{\partial C}{\partial x}\frac{\partial T}{\partial x} + \frac{\partial C}{\partial y}\frac{\partial T}{\partial y}\right) + \left(\frac{D_T}{T_c}\right)\left[\left(\frac{\partial T}{\partial x}\right)^2 + \left(\frac{\partial T}{\partial y}\right)^2\right] \tag{4}$$

**Nanoparticle conservation equation:**

$$u\frac{\partial C}{\partial x} + v\frac{\partial C}{\partial y} = D_B\left(\frac{\partial^2 C}{\partial x^2} + \frac{\partial^2 C}{\partial y^2}\right) + \frac{D_T}{T_C}\left(\frac{\partial^2 T}{\partial x^2} + \frac{\partial^2 T}{\partial y^2}\right) \tag{5}$$

The following dimensional boundary conditions have been assigned:

On top boundary: $u = v = 0$, $\frac{\partial T}{\partial y} = 0$, $\frac{\partial c}{\partial y} = 0$ (6a)

On bottom boundary: $u = v = 0$, $\frac{\partial T}{\partial y} = 0$, $\frac{\partial c}{\partial y} = 0$ (6b)

On left inclined boundary: $u = v = 0$,

$$T = T_c + (T_h - T_c)\,A\{sin(y - 0.3x) - x - 0.3y\}$$
$$C = C_c + (C_h - C_c)\,A\{sin(y - 0.3x) - x - 0.3y\} \tag{6c}$$

On right inclined boundary: $u = v = 0$,

$$T = T_c + (T_h - T_c)A\{sin(0.3x + y - 0.54) + 0.3y - x + 1.8\}$$
$$C = C_c + (C_h - C_c)A\{sin(0.3x + y - 0.54) + 0.3y - x + 1.8\} \tag{6d}$$

The thermal transport rate is computed at both inclined boundaries as they exist both cooling and heating conditions. The local Nusselt number expression is:

$$Nu = -\frac{hH}{k} = -\frac{\partial T}{\partial n}H \tag{7}$$

The transformation for converting dimensional equations into dimensionless form has been expressed as:

$$X = \frac{x}{H},\ Y = \frac{y}{H},\ U = \frac{uH}{\alpha},\ V = \frac{vH}{\alpha},\ P = \frac{uH^2}{\rho\alpha^2}, \theta = \frac{T - T_c}{T_h - T_c},\ \varphi = \frac{C - C_c}{C_h - C_c} \tag{8}$$

The dimensionless form of the equations (1) - (5) is:

$$\frac{\partial U}{\partial X} + \frac{\partial V}{\partial Y} = 0, \tag{9}$$

$$U\frac{\partial U}{\partial X} + V\frac{\partial U}{\partial Y} = -\frac{\partial P}{\partial X} + Pr\left(\frac{\partial^2 U}{\partial X^2} + \frac{\partial^2 U}{\partial Y^2}\right) \tag{10}$$

$$U\frac{\partial U}{\partial X} + V\frac{\partial V}{\partial Y} = -\frac{\partial P}{\partial Y} + Pr\left(\frac{\partial^2 V}{\partial X^2} + \frac{\partial^2 V}{\partial Y^2}\right) - Ra\,Pr\,Nr\,(\varphi - 1) + Ra\,Pr\,\theta, \tag{11}$$

$$U\frac{\partial \theta}{\partial X} + V\frac{\partial \theta}{\partial Y} = \frac{\partial^2 \theta}{\partial X^2} + Nb\left(\frac{\partial \varphi}{\partial X}\frac{\partial \theta}{\partial X} + \frac{\partial \varphi}{\partial Y}\frac{\partial \theta}{\partial Y}\right) + Nt\left[\left(\frac{\partial \theta}{\partial X}\right)^2 + \left(\frac{\partial \theta}{\partial Y}\right)^2\right] \tag{12}$$

$$U\frac{\partial \varphi}{\partial X} + V\frac{\partial \varphi}{\partial Y} = \frac{1}{Le}\left(\frac{\partial^2 \varphi}{\partial X^2} + \frac{\partial^2 \varphi}{\partial Y^2}\right) - \frac{Nt}{Nb\,Le}\left(\frac{\partial^2 \theta}{\partial X^2} + \frac{\partial^2 \theta}{\partial Y^2}\right) \tag{13}$$

Here $Pr = \frac{v_f}{\alpha_f}$, $Le = \frac{\alpha_f}{D_B}$, $Nt = \frac{D_T(\rho C)_p}{T_c(\rho c)_f}\frac{(\theta_h - \theta_c)}{\alpha_f}$, $Nb = D_B\frac{(\rho c)_p}{(\rho c)_f}\frac{(\varphi_h - \varphi_c)}{\alpha_f}$, $Nr = \frac{(\varphi_h - \varphi_c)(\rho_p - \rho_f)}{(1-\varphi_c)\rho_f(\theta_h - \theta_c)}$ and $Ra = \frac{g\beta(\theta_h - \theta_c)(1 - \varphi_c)H^3}{v_f^2}$ be the Prandtl number, Lewis number, thermophoresis, Brownian action, buoyancy relation and Rayleigh number, respectively.

And the non-dimensional boundary conditions are as follows:

On top boundary: $U = V = 0$, $\frac{\partial \theta}{\partial Y} = 0$, $\frac{\partial \varphi}{\partial Y} = 0$ (14a)

On bottom boundary: $U = V = 0$, $\frac{\partial \theta}{\partial Y} = 0$, $\frac{\partial \varphi}{\partial Y} = 0$ (14b)

On left inclined boundary: $U = V = 0$,

$$\theta = \varepsilon\{sin(Y - 0.3X) - X - 0.3Y\},$$
$$\varphi = \varepsilon\{sin(Y - 0.3X) - X - 0.3Y\} \tag{14c}$$

On right inclined boundary: $U = V = 0$,

$$\theta = \varepsilon\{sin(0.3X + Y - 0.54) - X + 0.3Y + 1.8\},$$

$$\varphi = \varepsilon\{sin(0.3X + Y - 0.54) - X + 0.3Y + 1.8\} \tag{14d}$$

The non-dimensional local Nusselt number at the inclined surfaces is:

$$\overline{Nu} = -\frac{\partial\theta}{\partial N}N \tag{15a}$$

The thermal gradient normal is:

$$\frac{\partial\theta}{\partial N} = \frac{1}{N}\sqrt{\left(\frac{\partial\theta}{\partial X}\right)^2 + \left(\frac{\partial\theta}{\partial Y}\right)^2} \tag{15b}$$

The mean Nusselt number at the inclined surfaces is:

$$Nu = -\frac{1}{N}\int_0^N \overline{Nu}dN \tag{15c}$$

## 4. Numerical Modeling

The FEM of Galerkin's residual technique [48] has been applied for solving the leading dimensionless PDEs (9-13) with boundary conditions (14a-d). Using FEM gridding the computational area is discretized into non-uniform finite number of elements ie. meshes. The pressure ($P$), concentration ($\varphi$), velocities ($U, V$), the heat ($\theta$) are dependent variables and Cartesian co-ordinates ($X, Y$) are independent variables. The velocity, temperature and concentration are associated with these six nodes but pressure is associated with only three corner nodes. The convergence measure for the resolution process is set as $|S^{m+1} - S^m| \leq 10^{-4}$, where $m$ and $S$ are the iteration number and function of all dependent variables. The detailing of this numerical technique has been described in (2021).

### 4.1 Code validation

For authentication of the results from present numerical technique, the obtained graphical representation of streamlines and isothermal lines are validated with that of Venkatadri *et al.* (2019). The code validation has been displayed by Figure 2. They simulated numerically free convective heat transfer 2D model of the trapezoidal cavity. At $Ra = 10^3$ and $Pr = 0.025$ this comparison has been conducted. A good quality of conformity is obtained in this validation technique. The authors become confident to run this code for the subsequent numerical results by producing this fine agreement.

### 4.2 Grid check

Table 1 displays a grid test which has been accomplished with different kind of meshes at $Pr = 7$, $Ra = 10^4$, $Nt = Nr = Nb = 0.1$ and $Le = 10$. The grid systems consist of nodes 4925, elements 1602, time 52s; nodes 7930, elements 2708, time 95s; nodes 20320, elements 2708, time 112s; nodes 49780, elements 18008, time 276s; and nodes 75500, elements 28296, time 403 s. After solving the governing equations, the obtained value of mean Nuselt number is chosen as the screening variable for this test. From the Table 1, it is noticed that no additional enhancement in the Nusselt number value occur with larger size of element. Considering the computational time and accuracy of numerical result of $Nu$, the present numerical simulation has been conducted with grid scheme of nodes 18082 and elements 4484.

Table 1: Grid test at $Pr = 7$, $Ra = 10^4$, $Nt = Nr = Nb = 0.1$ and $Le = 10$

| Element | 1602 | 2708 | 7142 | 18008 | 28296 |
|---------|------|------|------|-------|-------|
| *Nu* | 0.243 | 0.564 | 0.774 | 0.985 | 0.9854 |
| Time (s) | 52 | 95 | 112 | 276 | 403 |
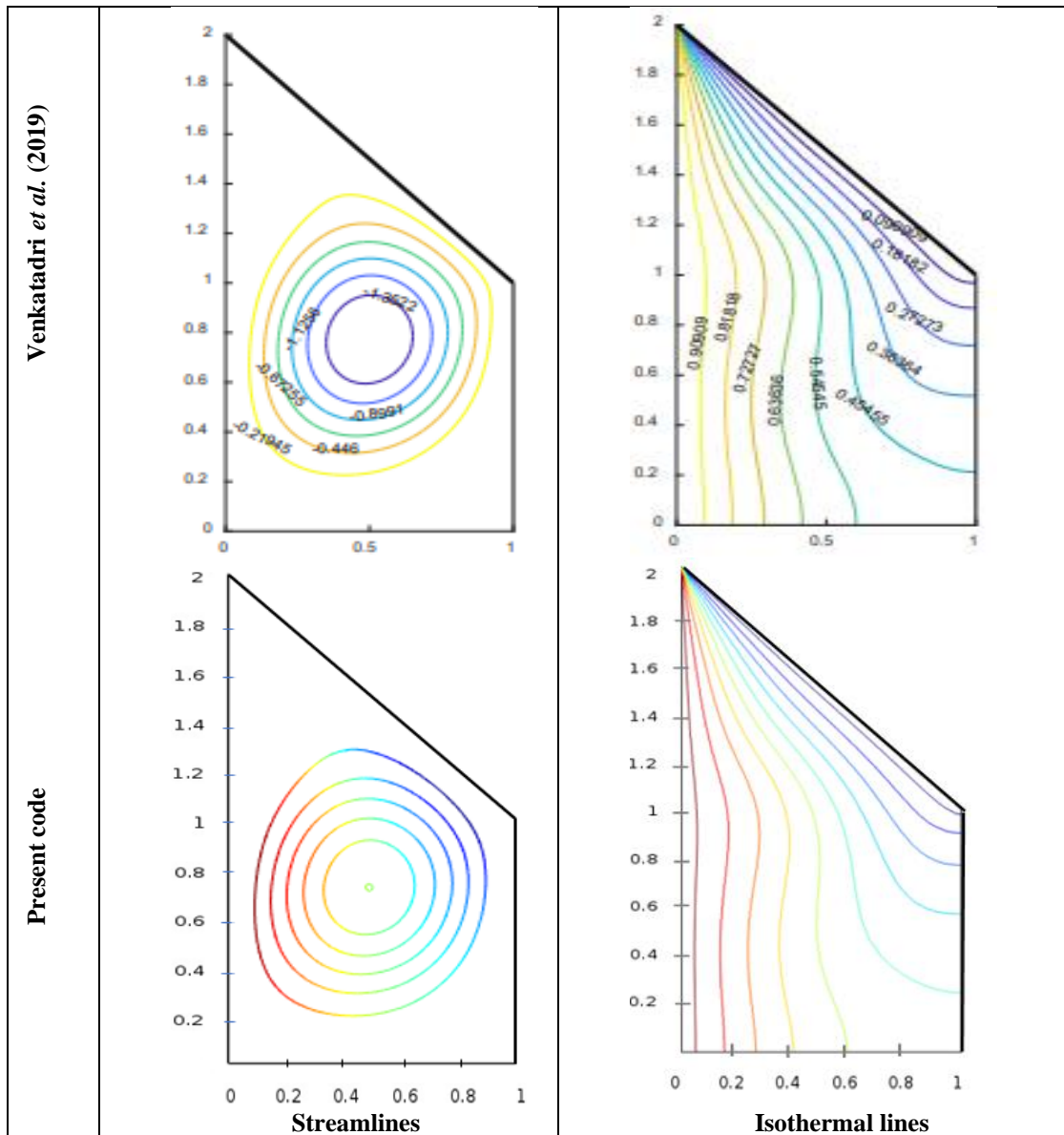
Figure 2: Justification of results from current model with Venkatadri *et al.* (2019) at $Ra = 10^3$ and $Pr = 0.025$

## 4.3 Finite element gridding

The FEM meshing of the computational domain of the present research has been depicted in Figure 3. The six nodes in a triangular shaped element are noticed all over the domain in this gridding system. The meshing is of non-uniform type.

## 5. Results and Discussion

Thermophoresis and Brownian action effects taking place the temperature, velocity as well as concentration has been identified. The flow, heat, and concentration fields for a specific temperature and material transfer application in a trapezium-shaped cavity have been obtained. Using Buongiorno's nanofluid a numerical modeling of free convection of thermal transport within a trapezoidal domain having periodic temperature and material allocations at the inclined boundaries is examined. The numerical calculation is carried out with Brownian action ($Nb$) from 0.1 to 2, Rayleigh number ($Ra$) from $10^3$ to $10^6$, thermophoresis ($Nt$) from 0.1 to 1.5, Prandtl number ($Pr$) from 0.7 to 10, Lewis number ($Le$) from 1 to 10 and buoyancy ratio ($Nr$) from 0.1 to 0.7. These relevant

parameters directly affect the velocity, thermal, and concentration fields within the considered domain. The results are offered in the form of streamlines, isothermal lines, nanoparticle volume fraction contours, and *Nu* on both inclined boundaries. To display the results, five parameters have been kept as fixed (unless where stated) out of these six independent parameters, while the single remainder one has been varied as gathered in the following categories:
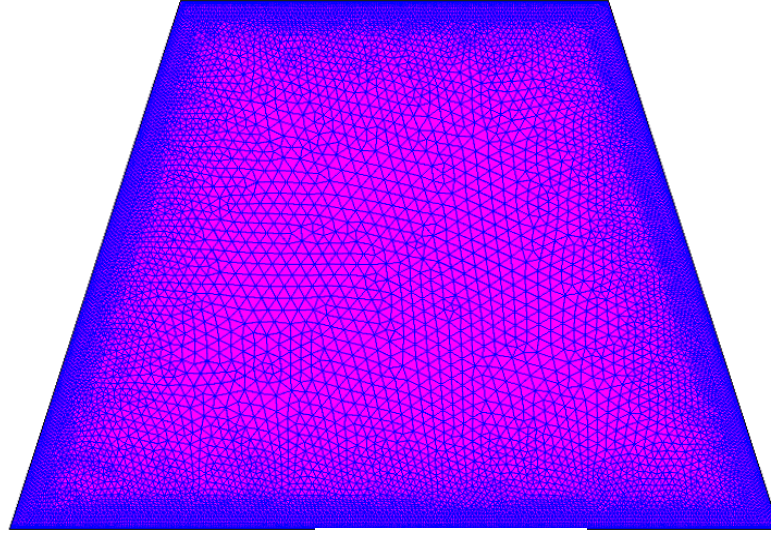


Figure 3: Gridding of the geometry

## 5.1 Effect of Lewis number

Figure 4 (a-c) illustrates the yielding of Lewis number on streamlines, isothermal lines, and iso-concentration lines in the range ($Le = 1 - 10$). For this effect the values of another parameter have been kept as fixed at $Pr = 7$, $Ra = 10^5$, $Nt = Nr = Nb = 0.1$. The blue colour indicates the lowest value, and the red colour represents the highest value in the streamlines, isothermal lines, and iso-concentration lines. It is noticed from this figure that an increase of Lewis number leads to both significant changes in the conservation of velocity, temperature, and nanofluid concentration fields. With the Lewis number, the non-convective cells are formed inside the cavity. The cells at the middle part vortices anticlockwise direction whereas the cells at top and bottom are vortices clockwise direction inside the enclosure of Figure 4 (a). The main reason for the emergence of these circulations is the sinusoidal temperature distribution on the inclined wall. The vortices are partitioned by the virtual horizontal and inclined walls, which are both waterproof and adiabatic. Non-convective cells are approaching the vertical wall due to great temperature variations in this zone. The figure shows that the intensity at the middle part is greater than the intensity at the top and bottom parts inside the cavity.

It is also seen from Figure 4 (b) that the non-convective cell cores are approaching the vertical walls due to significant temperature differences in these zones. An enhancement of Lewis number does not change in all endemic fields of the temperature inside the cavity. It physically refers to that flow with a large Lewis number hamper extending nanoparticles in the nanofluid. Therefore, we get large uniform areas in the domain of consecutive cells. The only non-homogeneous place determined at $Le = 7$.

At $Le \leq 10$, the ordination of nanoparticles is non-uniform. It physically means that leads to spreading nanoparticles in the nanofluid. Therefore, we get a sizeable non-uniform place in the state of convective cells. Figure 4 (c) shows the main variations with the Lewis number related to the iso-concentrations. These fields characterize the allocation of the nanoparticle volume fraction into the trapezoidal enclosure.

The dimensionless Lewis number on the average Nusselt number at left and right inclined walls is presented in Figure 5. This figure shows that an increase in $Le$ from 1 to 10 leads to a significant enhancement in the average Nusselt number at the left and right inclined wall. The increasing average Nusselt numbers at the right and left walls are 0.7108 and 0.7081%. The growing rate of the average Nusselt number with Lewis's number at the right wall is greater than the left wall. The ever-increasing rate is 0.3813% greater at the right wall than the left wall. When the Lewis number varies from 1 to 4 the temperature highly increases. For the Lewis numbers 1, 4, 7, and 10, we get the numerical value of Nusselt numbers 6.049, 6.077, 6.087, and 6.092, respectively at the left wall

and 6.072, 6.1, 6.11, and 6.115, respectively on the right wall. From the figure, we see that the temperature increasing rate is higher for lower *Le* and increases parallelly for both partitions.
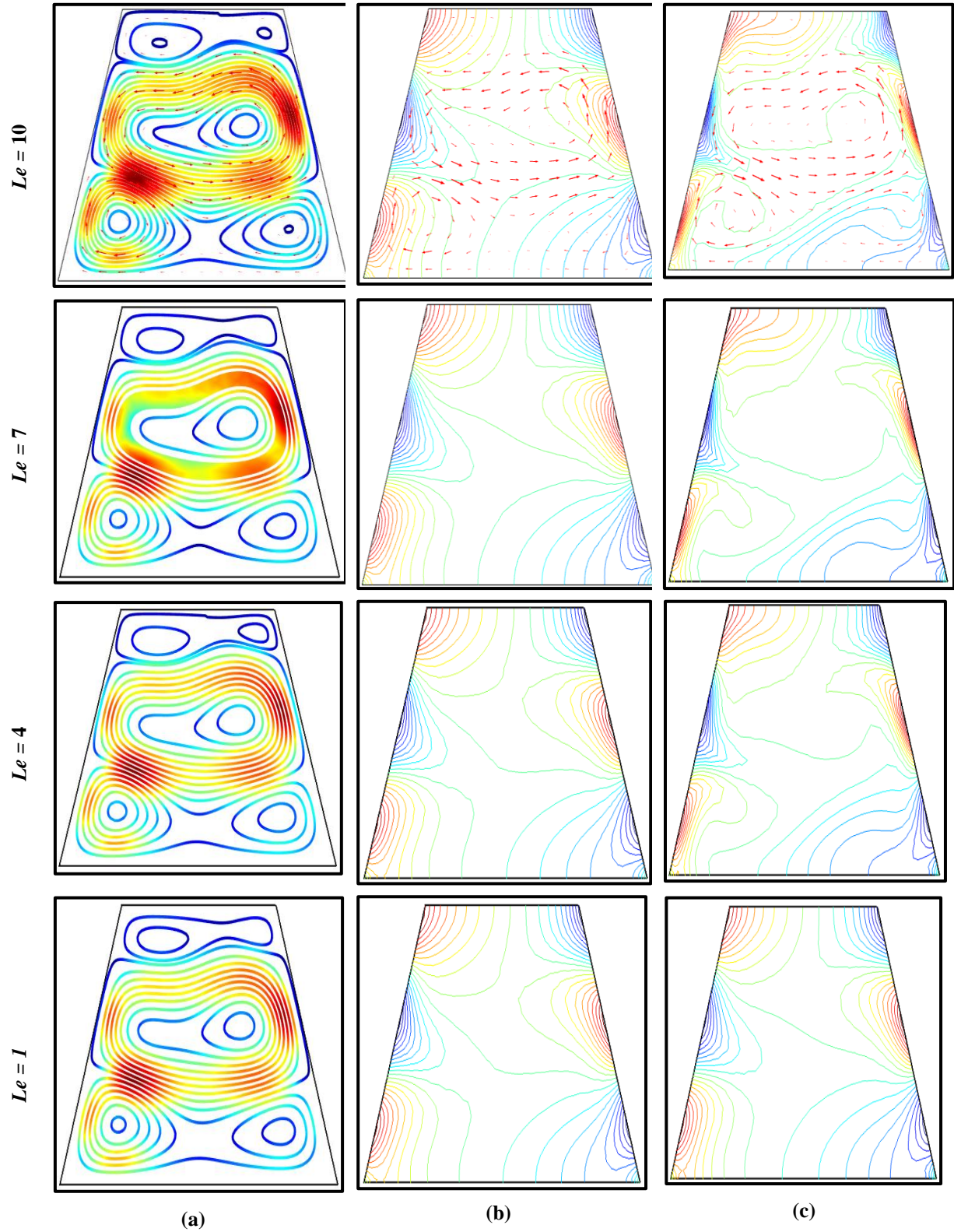


Figure 4: *Le* effect on (a) streamlines, (b) isothermal lines and (c) iso-concentrations with $Pr = 7$, $Ra = 10^4$, $Nt = Nr = Nb = 0.1$
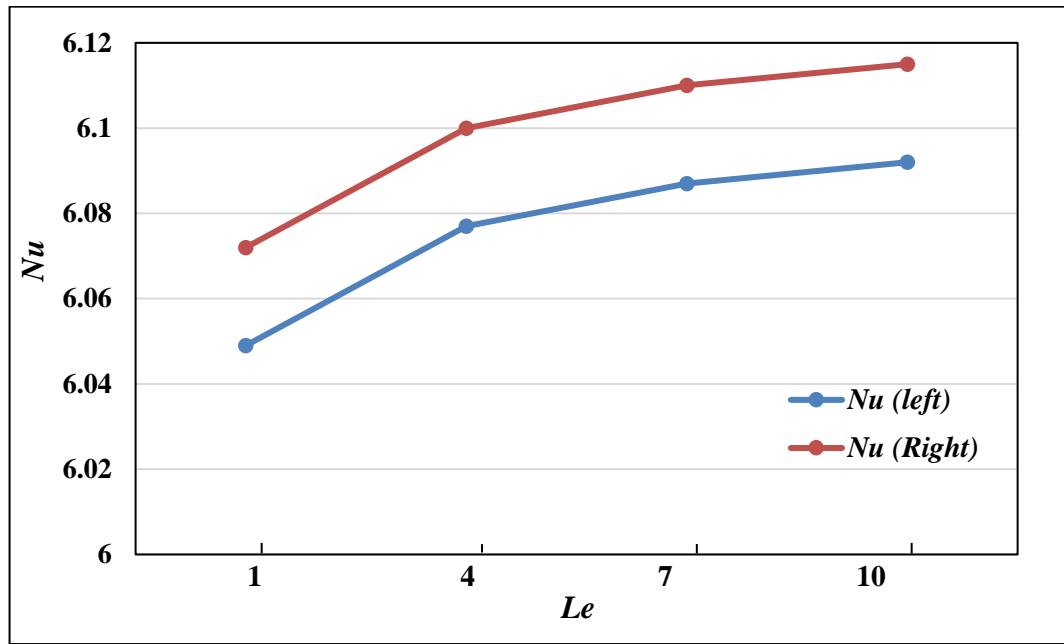
Figure 5: *Nu* at inclined boundaries against *Le* with *Pr* = 7, *Ra* = $10^4$, *Nt* = *Nr* = *Nb* = 0.1

## 5.2 Effect of thermophoresis

Figures 6 (a-c) illustrate the effect of thermophoresis parameter (*Nt*) from 0.1 to 1.5 on the temperature, velocity, and nanoparticle concentration contours with fixed *Le* = 10, *Pr* = 7, *Ra* = $10^5$, *Nr* = *Nb* = 0.1. The non-convective cells are formed in both clockwise and anticlockwise directions along the streamlines inside the cavity. An enhancement in *Nt* governance the alteration in all characteristics (streamlines, isotherms and iso-concentrations). Regardless of the thermophoresis, there is a small but significant change in streamlines.

The figure shows the intensification and increment in size at the bottom part and attenuation and decreases in size in the upper part of the enclosure. The shape of primary cells on the middle side has been changed slightly due to an increase in *Nt*. It is essential to notice a significant change in an oval shape at the top side. The elliptical shape core at the top has been smaller than the before condition. At the same time, it is observed from Figure 6 (b) that an increase in thermophoresis parameter leads to more intensive heating of the bottom part than the upper part of the enclosure. Such changes characterize a decrease in temperature differences in the bottom part and an increase in temperature difference at the upper part.

It is noticed from Figure 6 (c) that the principal variations due to thermophoresis parameters are involved in the iso-concentrations. For example, an increase in *Nt* leads to essential nanoparticle volume fraction changes in the cavity's upper and bottom parts. In general, these allocations are considered non-uniform.

The average Nusselt number due to the thermophoresis parameter at the left and the right inclined wall is delineated in Figure 7. It is necessary to note that an increase in *Nt* leads to an increase in the average Nusselt number. The figure shows that the rise in the average Nusselt number at the right wall is 34.75 and at the left wall is 34.50% for *Nt* = 0.1 to *Nt* = 1.5. Thus, the average Nusselt number at the right border is higher than the left wall, and the increasing rate at the right wall is *Nt* = 0.724% compared with the left wall.

## 5.3 Effect of Prandtl number

Figure 8 (a-c) displays the effect of Prandtl number from 0.7 to 10 on velocity, temperature and concentration contours with fixed *Ra* = $10^5$, *Nt* = *Nr* = *Nb* = 0.1 and *Le* = 10. From the streamline's contours, it is found that there is a small change in the convective cell. For *Pr* = 0.7, the primary elliptic circulation cells and small oval shape core have been created. At *Pr* = 4, the shape of the primary cell remains the same, but the oval shape at the top side has been changed a little bit and it is important to notice that the oval shape core at the top has been less than the before shape. On the other hand, when *Pr* = 7 and *Pr* = 10, there is little distinction in the streamlines that gradually increment of oval shape core. There is little change in the isotherm.
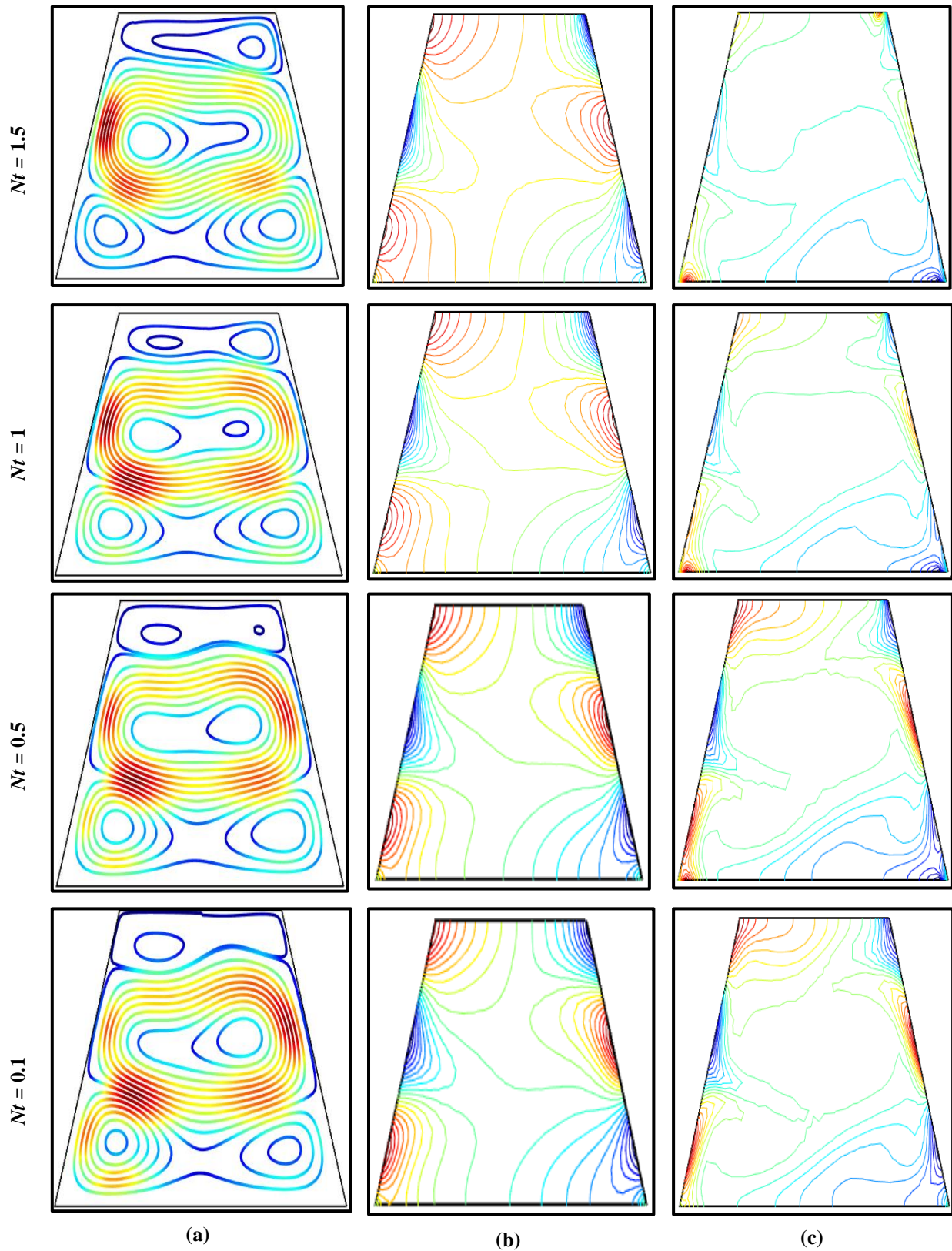
Figure 6: Thermophoresis effect on (a) velocity, (b) temperature and (c) concentration contours with $Le = 10$, $Pr = 7$, $Ra = 10^4$, $Nr = Nb = 0.1$
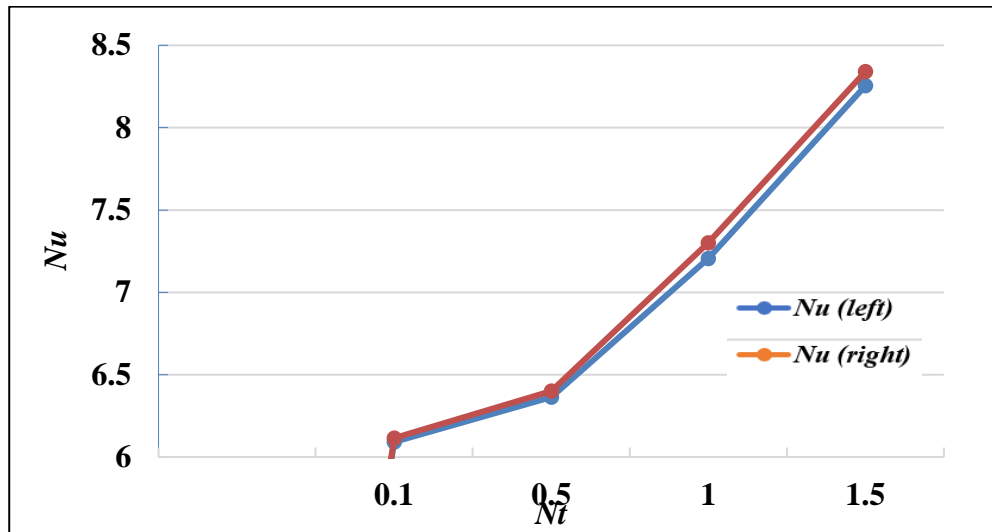
Figure 7: *Nu* at inclined walls against *Nt* with *Le = 10, Pr = 7, Ra = 10$^4$, Nr = Nb = 0.1*

One crucial thing is noticed from Figure 8 (b) that an increment in *Pr* guides to an augmentation in the intensity of non-convective cell inside the cavity. Thus, the passion is higher at both base, and upper part of left boundary, whereas the power is more elevated at the middle part for the right wall.

Figure 8 (c) depicts the principal variations with the Prandtl number (*Pr*) concerned with the iso-concentrations. Rising *Pr* guides to necessary nanoparticle concentration changes at the top and base portions of the domain. Therefore, these allocations may not be assumed as homogeneous.

The Prandtl number (*Pr*) effect on the average Nusselt number at left and right inclined walls is presented in Figure 9. An increase in the Prandtl number from 0.7 - 4 leads to a high rise in the average Nusselt number but from 4-10 leads to slight growth in the average Nusselt number. The average increase in Nusselt number due to the Prandtl number at the right wall is 0.4104 and the left wall 0.893%. This calculation shows that the average increase in Nusselt number due to the Prandtl number at the right inclined wall is more significant than the left wall. Due to *Pr* (0.7, 4, 7, and 10), the values of *Nu* at the right wall are 6.091, 6.113, 6.115, and 6.116 and at the border are 6.039, 6.087, 6.092, and 6.093, respectively. The temperature variation gradually increases with both the increase of *Pr*.

## 5.4 Effect of Brownian motion

Figure 10 (a-c) illustrates Brownian motion's effect on streamlines, isothermal lines, and iso-concentration lines in the range (*Nb* = 0.1 - 2.0). For this effect the values of another parameter have been kept as fixed at *Pr = 7, Le = 10, Ra = 10$^5$, Nt = Nr = 0.1* and. It is noticed from the figure that there is a significant change among the temperature, velocity conservation and nanofluid concentration fields for enhancing Brownian action. This parameter forms non-convective cells along streamlines in both clockwise and anticlockwise directions inside the enclosure of Figure 10 (a). The primary reason for this circulation is the sine wavy temperature ordination at inclined walls of the cavity. A waterproof and adiabatic wall separates the vortices.

With an increase of the Brownian motion parameter, there is a slight change in severity and configuration in the streamlines and isotherms. According to Figure 10 (b), an enhancement of *Nb* leads to the homogeneity of distribution inside the cavity. It is also noticed that the temperature variation is increased both in the top and bottom part with the increased Brownian motion parameter.

A significant variation in iso-concentration with the Brownian motion parameter is found in Figure 10 (c). An increment of *Nb* changes nanoparticle volume fractions essentially in the upper and bottom parts of the enclosure. Therefore, these distributions can be thought non-homogeneous.
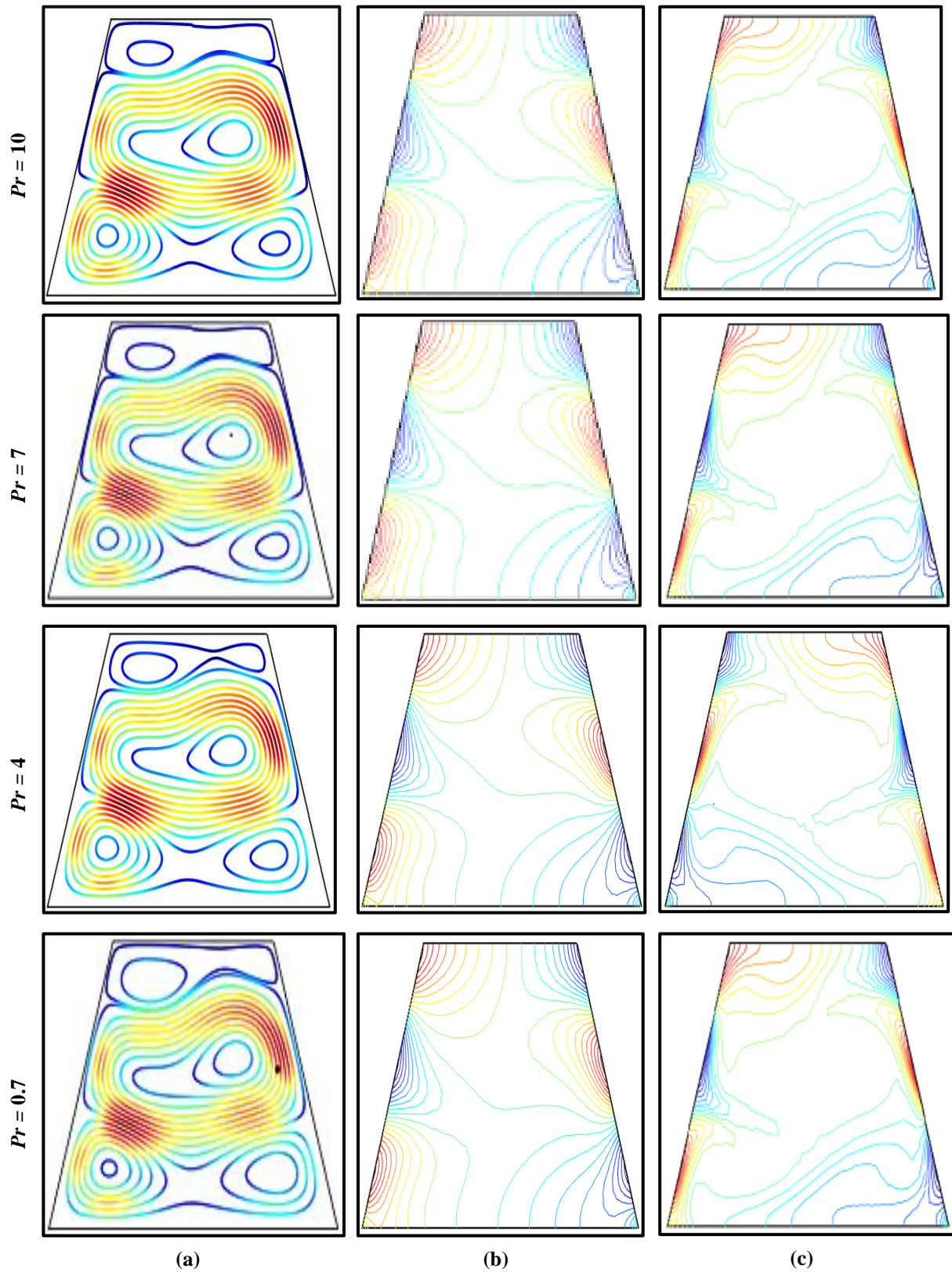
Figure 8: *Pr* effect on (a) velocity, (b) temperature and (c) concentration contours with $Ra = 10^4$, $Nt = Nr = Nb = 0.1$ and $Le = 10$
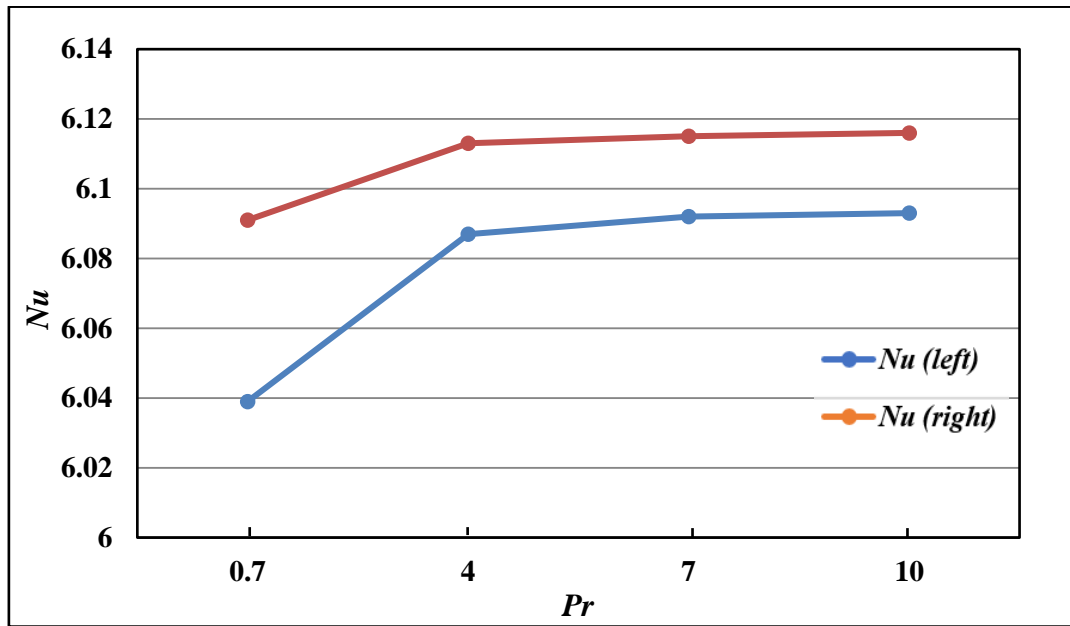
Figure 9: *Nu* at inclined boundaries against *Pr* with *Le* = 10, *Ra* = $10^4$, *Nt* = *Nr* = *Nb* = 0.1

The Brownian motion parameter's (*Nb*) effect on the average Nusselt number in both inclined walls is presented in Figure 11. Variation of *Nb* from 0.1 - 2 leads to a growth in the average Nusselt number on both ready walls. However, the average increase in Nusselt number due to the *Nb* parameter at the right wall is more significant than the left wall. The increasing average Nusselt number is approximately 34.75% and 34.27% for the right and left borders, respectively, for rising values of Brownian motion. After calculation, the average Nusselt number 1.40% higher for the right wall than the left wall. There is a linearity of increase in temperature against the Brownian motion number at both left and right wall.

## 5.5 Effect of buoyancy ratio

Figure 12 (a-c) illustrates the buoyancy ratio effects on streamlines, isothermal lines, and iso-concentration lines in the range (*Nr* = 0.1- 0.7). For this effect the values of another parameter have been kept as fixed at *Le* = 10, *Pr* = 7, *Nt* = *Nr* = 0.1 and *Ra* = $10^4$. It is noticed from this figure that rising buoyancy proportion guides to both significant changes in the conservation of velocity, temperature, and nanofluid concentration fields. The non-convective cells are formed in the streamlines along the anticlockwise direction inside the cavity of Figure 12 (a) with a buoyancy ratio. There is a significant change in both the primary and oval shapes. The primary shape at *Nr* = 0.3 is bent through a little bit than the last cells. Finally, the cells turned into a circular shape. The oval contour shape at the top and bottom part gradually decreases with the increment in buoyancy ratio.

Non-convective cells are close to the inclined wall due to the significant temperature difference in this zone of Figure 12 (b). With an increase of the buoyancy ratio parameter, there is a slight change in intensity and configuration in the isotherm. The enrichment of the thermal conductivity produces denser isotherms which is the indication of the transfer of temperature. Figure 12 (b) shows that the increase in the value of *Nr* weak the isothermal lines.

The increase in *Nr* iso-concentration lines characterizes a reduction in nanoparticle solid concentration near the top and a rise near the bottom part of Figure 12 (c). That is, the material allocations of Buongiorno's nanofluid retard as buoyancy proportion becomes higher.

The buoyancy ratio (*Nr*) effect on *Nu* at the both inclined boundaries is presented in Figure 13. An increment in *Nr* from 0.1- 0.7 guides to a significant reduction in the thermal transport rate. The average decrease in Nusselt number due to *Nr* along the right inclined boundary is more important compared with left boundary. The decreasing rates of the left and right borders are 1.101 and 1.104%, respectively. Decreasing rate at the right wall compared with the left wall is 0.272%.
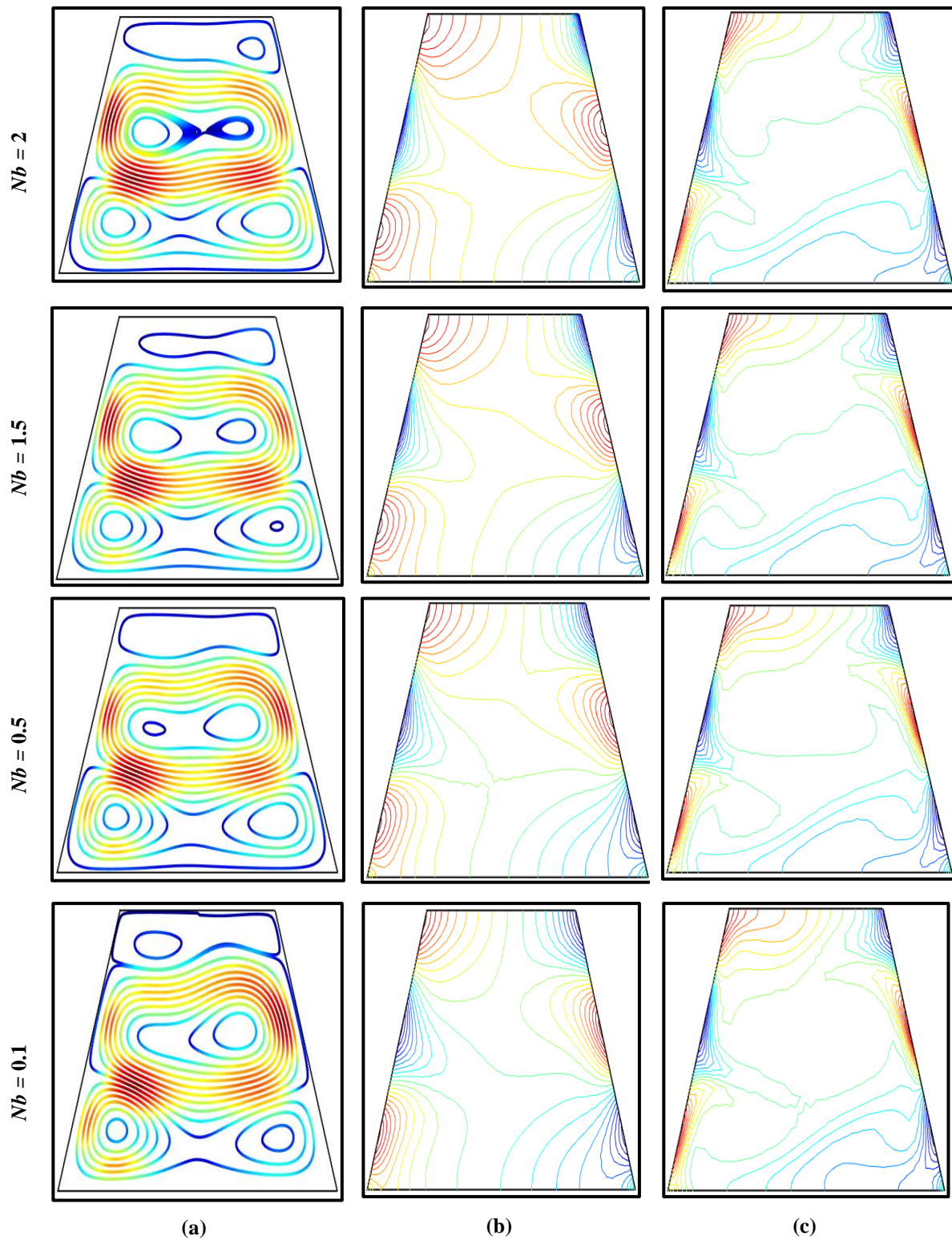
Figure 10: Brownian motion effect on (a) velocity, (b) temperature and (c) concentration contours with $Pr = 7$, $Ra = 10^4$, $Nt = Nr = 0.1$ and $Le = 10$
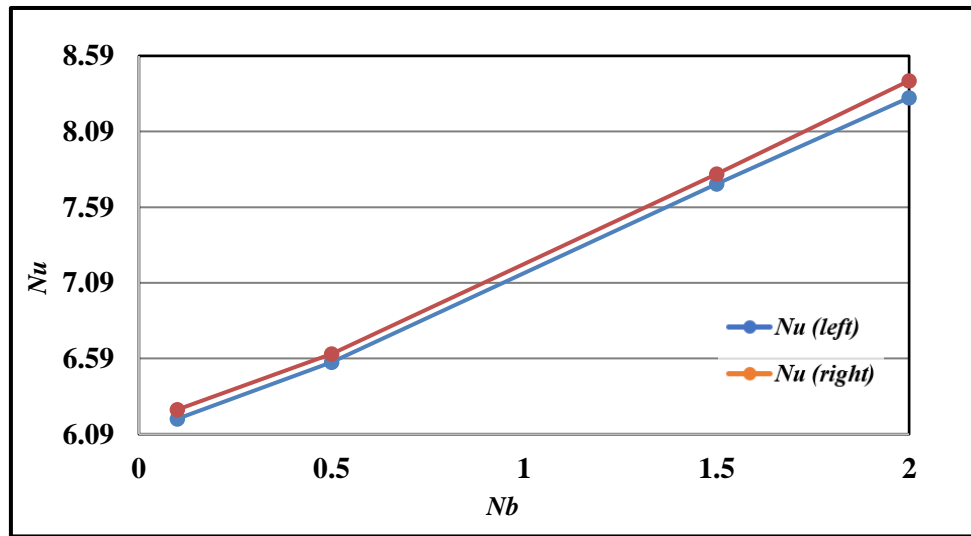
Figure 11: *Nu* against Brownian motion with *Pr* = 7, *Ra* = $10^4$, *Nt = Nr* = 0.1, *Le* = 10

## 5.6 Effect of Rayleigh number

Figure 14 (a-c) illustrate the outcomes of buoyancy force on velocity, temperature and concentration contours in the range (*Ra* = $10^3$- $10^6$). For this effect the values of another parameter have been kept as fixed at *Pr* = 7, *Nt = Nr = Nb* = 0.1 and *Le* = 10. in spite of the buoyancy force the non-convective vortices are observed in the velocity contour along the clockwise track of Figure 14 (a).

The major cause for the manifestation of these rotations is the result of the sinusoidal temperature distribution at vertical walls of the cavity. The circular cells in Figure 14 (b) are alienated by implicit horizontal and inclined wall which are both insulated and impermeable. It can be seen from figure that there is a significant change in both the primary cells and in oval contour shape at the top side. The strength of major vortices diminishes for rising *Ra*. The primary cells become compressed for escalating buoyancy force and finally turned into rectangular shape. On the other hand, the oval is large and circular in shape at bottom become thin at top side at the lowest value of *Ra*. But we noticed that enhancing buoyancy force, the oval at the bottom gets smaller, and the top gets larger gradually. There is a slight change in intensity and configuration in the isotherm with a rise in Rayleigh's number. We noticed that the curve in the isotherm contour inversely changed between *Ra* = $10^3$ and *Ra* = $10^4$. The isothermal lines scatter haphazardly at *Ra* = $10^6$ and these distributions can be concentrated as non-homogeneous.

The variation with the Rayleigh number is related to the iso-concentration lines, as shown in Figure 14 (c). Curve close to the inclined wall due to significant temperature difference in this zone. At *Ra* = $10^3$, all carves are close to each other and stay in a chaplet. This chaplet shape demolishes with the growth of buoyancy force. Finally, the curves arrange parallel for the highest *Ra*.

The Rayleigh number (*Ra*) effect on *Nu* along the left and right inclined boundaries is presented in Figure 15. From the diagram below, we conclude that an increment of Rayleigh number (*Ra*) from *Ra* = $10^3$ – $10^5$ shows hardly any increase in the rate of heat transport. But *Ra* from $10^5$ to $10^6$, *Nu* rises highly for both inclined boundaries. Increasing rates of heat transfer are 36.193 and 35.988% for right and left borders, respectively. In addition, about 0.5696% enhanced thermal transport rate is obtained along right wall judged against to left wall. The numerical value of *Nu* obtained at the left and right wall be 5.763, 5.765, 6.159, 7.783, and 5.79, 5.8, 6.159,7.895, respectively. The more excellent value of the Rayleigh number leads to an increase in temperature highly. After analyzing the data value, we conclude that the increasing rate of temperature for both walls is very close.
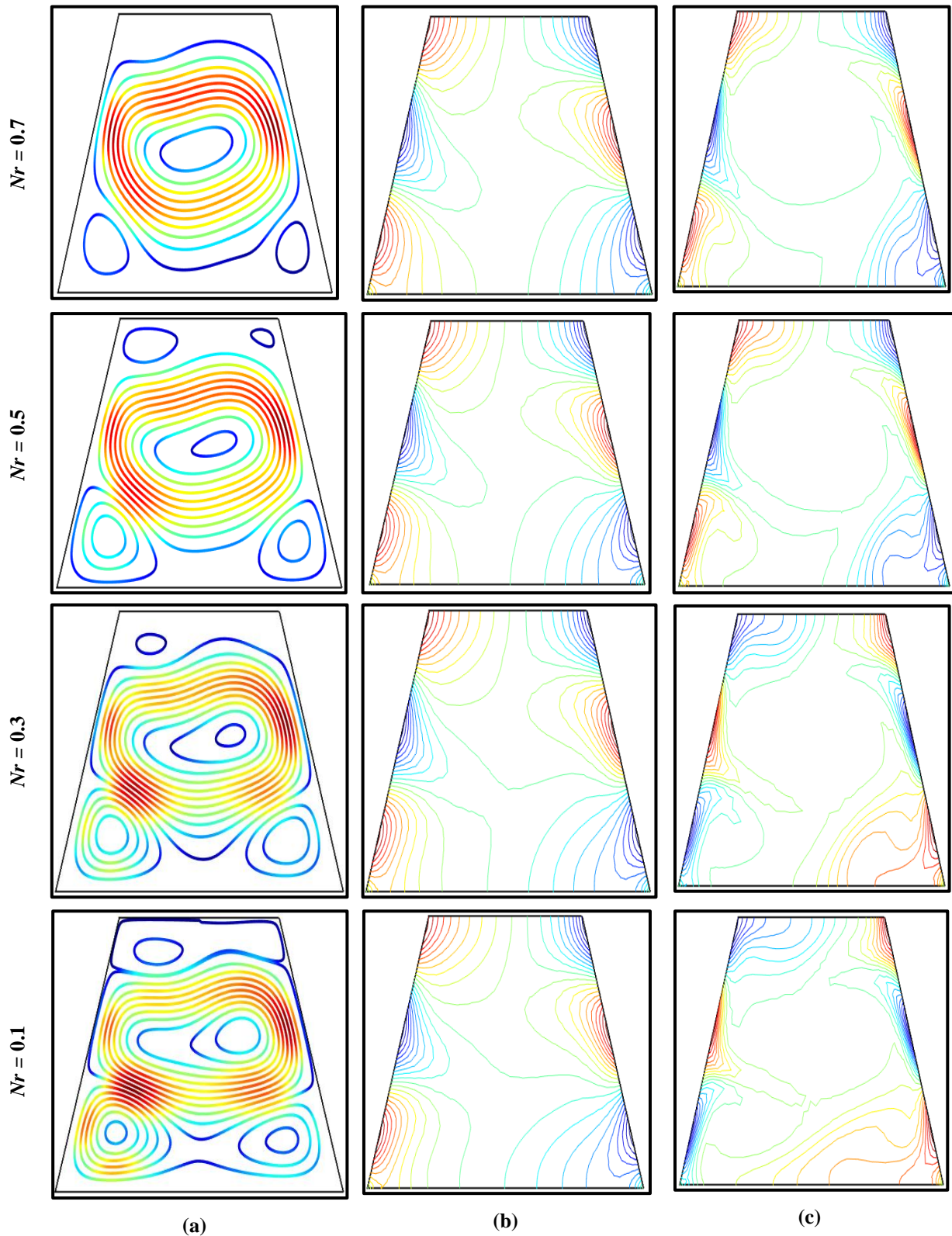
Figure 12: *Nr* effect on (a) velocity, (b) temperature and (c) concentration contours with $Pr = 7$, $Ra = 10^4$, $Nt = Nb = 0.1$ and $Le = 10$
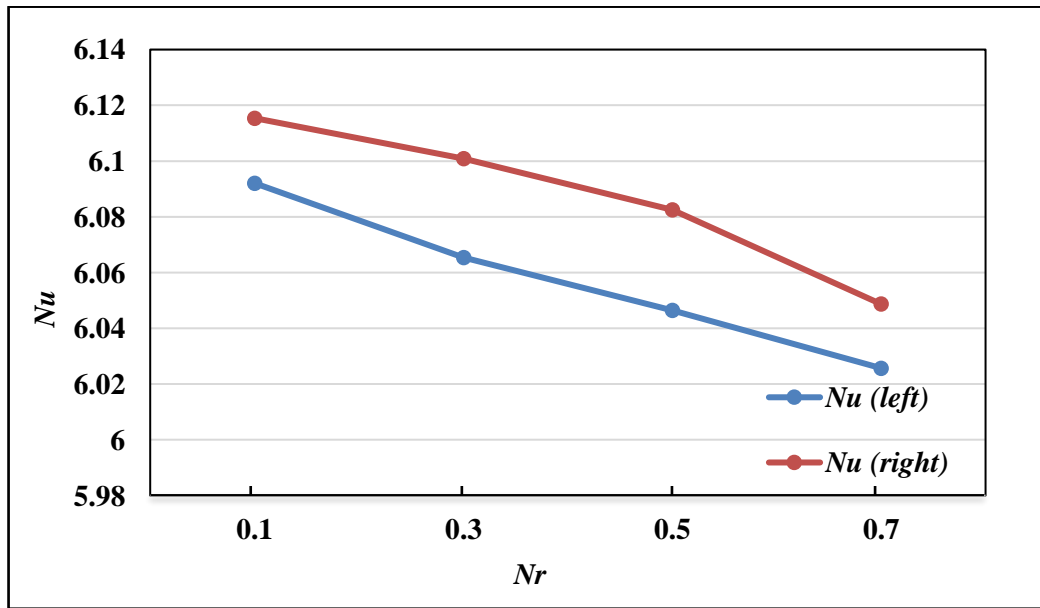
Figure 13: Nu against buoyancy ratio with $Le = 10$, $Ra = 10^4$, $Pr = 7$ and $Nb = 0.1 = Nt$

Three simplified test problems have been selected for comparison, such as Revnic *et al.* (2019) of non-uniform boundary heat variation on unsteady natural convective nanofluid flow in a trapezium, Demirdzic *et al.* (1992) of convective thermal transport inside a parallelogram and De Vahl Davis (1983) of free convective temperature movement within a square domain. *Nu* for interpreting Prandtl as well as Rayleigh numbers has been compared with that of the studies above. Table 2 presents values of *Nu* along with the heating halves of both inclined walls against *Pr* with fixed $Ra = 10^6$ and the percentage of error between the present result and that of Revnic *et al.* (2019). Thus, an excellent agreement has been observed among the current result with Demirdzic *et al.* (1992) and Revnic *et al.* (2019). At this time, the effects of the other parameters have been considered negligible for assimilation.

Table 2: Comparison of *Nu* against *Pr* among present result and that of Demirdzic *et al.* (1992) and Revnic *et al.* (2019)

| *Pr* | *Nu* | | | Error (%) |
|---|---|---|---|---|
| | **Demirdzic *et al.* (1992)** | **Revnic *et al.* (2019)** | **Present result** | |
| 0.1 | 5.9849 | 5.9829 | 6.3568 | 6.25 |
| 10 | 7.5801 | 7.5847 | 8.0932 | 6.70 |

Similarly, Table 3 presents values of *Nu* along with the heating halves of both inclined walls against *Ra* with fixed $Pr = 0.1$ and the percentage of error between the present result and that of Revnic *et al.* (2019). From Table 3, it is seen that a small amount of error is found between the current influence and that of Revnic *et al.* (2019). In this case, an excellent agreement has also been found among the present result with Davis and Jones (1983) and Revnic *et al.* (2019).

**(a)**          **(b)**          **(c)**
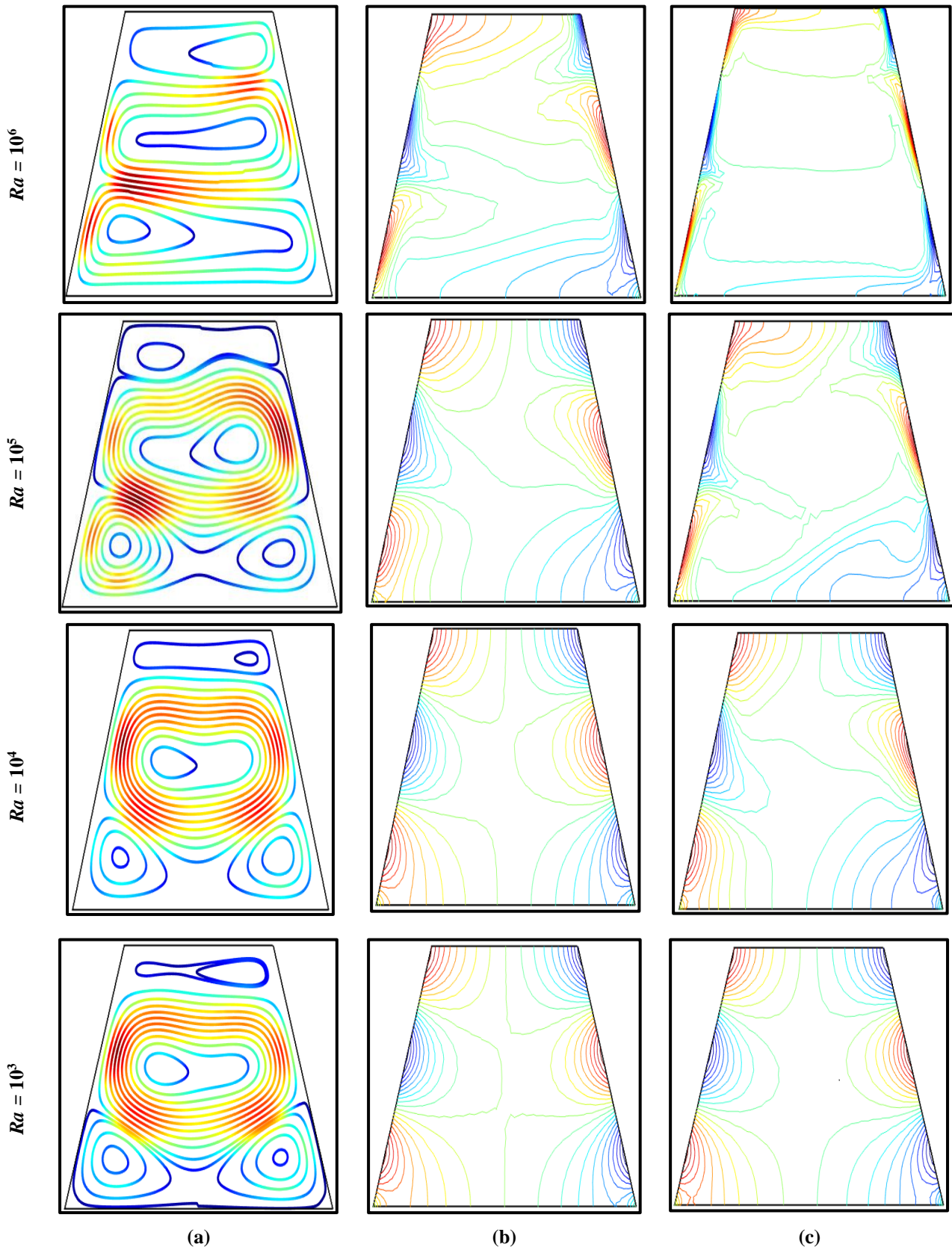
Figure 14: *Ra* effect on (a) velocity, (b) temperature and (c) concentration contours with *Pr* = 7, *Nt* = *Nr* = *Nb* = 0.1 and *Le* = 10
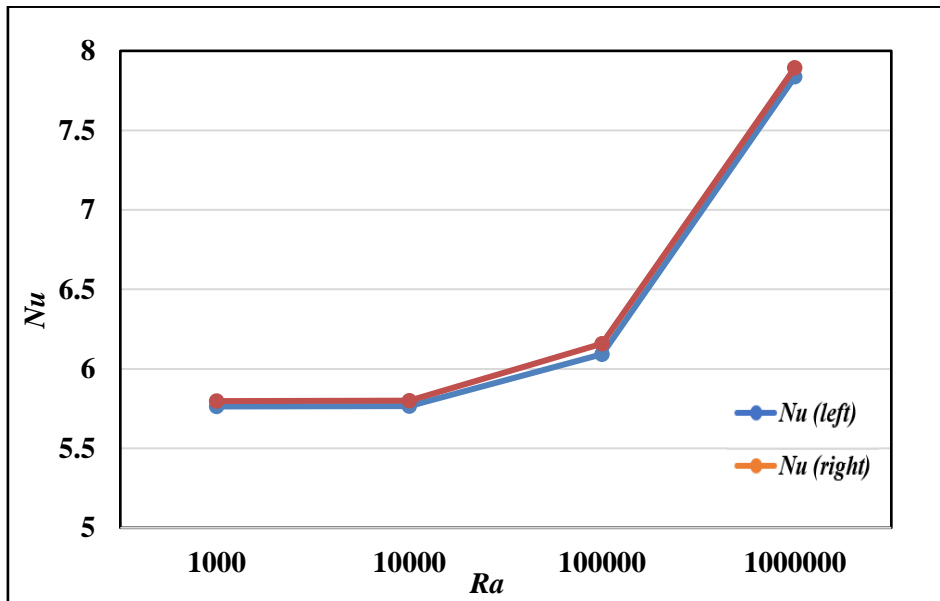
Figure 15: *Nu* at the inclined boundaries against *Ra* with *Le* = 10, *Ra* = $10^4$ and *Nt* = *Nr* = *Nb* = 0.1

## 5.7 Comparison

Table 3: Comparison of Nu against *Ra* among present result and that of Davis and Jones (1983) and Revnic *et al.* (2019)

| *Ra* | *Nu* | | | Error (%) |
|---|---|---|---|---|
| | **Davis and Jones (1983)** | **Revnic *et al.* (2019)** | **Present result** | |
| $10^3$ | 1.116 | 1.121 | 1.189 | 6.06 |
| $10^4$ | 2.234 | 2.306 | 2.401 | 4.12 |

## 6. Conclusions

The allocation of velocity, temperature and material contours with a comprehensive range of basic considerations has been investigated. From this numerical modeling, it is noticed that *Nu* is a growing function of thermophoresis, Lewis number, and Brownian action, whereas the decreasing relation of buoyancy proportion. Furthermore, comparisons of the result from this numerical study have also been performed with other numerical/experimental studies, and the comparisons are in excellent agreement. Therefore, the main findings of the present research have been enlisted as:

➢ *Nu* is obtained approximately 0.7108 and 0.7081% along the right and left border, respectively, to increase Lewis number values from 1 to 10. Thus, the increasing rate is 0.38% higher for the right wall than the left inclined wall.

➢ The heat transfer rate increases significantly by 34.50% and 34.75% in both left and right walls, respectively, with the thermophoresis from 0.1 to 1.5. Thus, *Nu* along the right boundary is 0.73% higher than left boundary.

➢ The rate thermal transport is attained about 0.41% and 0.89% for both inclined boundaries due to increasing Prandtl number from 0.7 to 10.

➢ Variation of Brownian motion number *Nb* from 0.1 to 2 guides for enhancement in the rate of temperature transport of 34.75 and 34.27% for the right and left fences, respectively. In addition, *Nu* is getting higher, about 1.40% for the right wall compared with the left wall.

➢ *Nu* decreases with the increasing values of *Nr*. Therefore, the decreasing rates at the right and left boundaries are approximately 1.104 and 1.101%, respectively. After calculation, the decreasing rate of *Nu* along right boundary compared with left boundary is found as 0.27%.

➢ Variation of Rayleigh's number from $Ra = 10^2$ to $10^6$ conducts a significant increase in heat translation at 36.19% and 35.99% for both right and left walls, respectively. In addition, the heat translation rate is 0.57% higher for the right wall than the left wall.

**References**

Elshehabey, H.M., and Ahmed, S.E. (2015): MHD mixed convection in a lid-driven cavity filled by a nanofluid with sinusoidal temperature distribution on the both vertical walls using Buongiornor's nanofluid model, International Journal of Heat and Mass Transfer, Vol. 88, pp. 181-202. https://doi.org/10.1016/j.ijheatmasstransfer.2015.04.039.

Sheikholeslami, M., Gorji-Bandpy, M., Ganji, D.D., Rana, P., and Soleimani, S. (2014): Magneto hydrodynamic free convection of $Al_2O_3$-water nanofluid considering thermophoresis and Brownian effects, Computer and Fluids, Vol. 94, pp.147-160. https://doi.org/10.1016/j.compfluid.2014.01.036.

Suriyakumar, P., and Devi, A. (2019): Buongiorno Model for hydromagnetic convection flow of nanofluid over an inclined stretching surface with variable stream conditions, Journal of Advanced Research in Applied Mechanics and Computational Fluid Dynamics, Vol. 6, pp. 1-14. https://orcid.org/0000-0003-0496-5582.

Falana, A., Ojewale, O.A., and Adeboje, T.B. (2016): Effect of Brownian motion and thermophoresis on a nonlinearly stretching permeable sheet in a nanofluid, Advances in Nanoparticles, Vol. 5, pp. 123-134. http://dx.*doi.org*/10.1016/j.icheatmasstransfer.2010.06.004.

Revnic, C., Ghalambaz, M., Grosan, T., Sheremet, M., and Pop, I. (2019): Impact of non-uniform border temperature variations on time-dependent nanofluid free convection within a trapezium: Buongiorno's nanofluid model, Energies, Vol. 12, pp. 1-14. https://doi.org/10.3390/en12081461.

Esfandiary, A., Mehmandoust, B., Karimipour, A., and Pakravan, H.A. (2016): Natural convection of $Al_2O_3$-water nanofluid in an inclined enclosure with the effect of slip velocity mechanism: Brownian motion and thermophoresis phenomenon, International Journal of Thermal Sciences, Vol. 105, pp. 137-158. https://doi.org/10.1016/j.ijthermalsci.2016.02.006.

Zargartalebi, H., Ghalambaz, M., Noghrehabadi, A., and Chamkha, A. (2016): Natural convection in an enclosure within inclined local thermal non-equilibrium porous fin considering Buongiorno's model, An International Journal of Computer and Methodology, Vol. 70, pp. 432-445. https://doi.org/10.1080/10407782.2016.1173483.

Alam, S., Sarower, F., Rahman, M.M., and Uddin, M.J. (2015): Effect of thermophoresis and Brownian motion on unsteady forced convection flow of a nanofluid along a porous wedge with variable suction, Bulletin of Calcutta Mathematical Society, Vol. 107, pp. 393-410. https://www.researchgate.net/publication/292736020.

Samimi Behbahan, A. A., and Pop, I. (2015): Thermophoresis and Brownian effects on natural convection of nanofluids in a square enclosure with two pairs of heat source/sink, International Journal of Numerical Methods for Heat & Fluid Flow, Vol. 25, pp. 1030-1046. https://doi.org/10.1108/HFF-05-2014-0134.

Sheremet, M.A., Grosan and Pop, I. (2014): Free convection in a shallow and slender porous cavity filled by a nanofluids using Buongiorno's model, ASME Journal of Heat Transfer, Vol. 136, pp. 082-501. https://doi.org/10.1115/1.4027355.

Elshehabey, H.M., and Ahmed, S.E. (2015): MHD mixed convection in a lid driven cavity filled a nanofluid with sinusoidal temperature distribution on the vertical walls using Buongiorno's nanofluid model, International Journal of Heat and Mass Transfer, Vol. 88, pp. 181-202. https://doi.org/10.1016/j.ijheatmasstransfer.2015.04.039.

Haddad, Z., Abu-nadac, E., Oztop, H.F., and Mataoui, A. (2012): Natural convection in nanofluids: are the thermophoresis and Brownian motion effects significant in nanofluid heat transfer enhancement, International Journal of Thermal Sciences, Vol. 57, pp. 152-162. https://doi.org/10.1016/j.ijthermalsci.2012.01.016.

Matin, M.H., and Ghanbari, B. (2014): Effect of Brownian motion and thermophoresis on the mixed convection of nanofluid in a porous channel including flow reversal, Transport in Porous Media, Vol. 101, pp. 115-136. https://doi.org/10.1007/s11242-013-0235-x.

Aminfar, H., and Haghgoo, M.R. (2012): Brownian motion and thermophoresis effects on natural convection of alumina-water nanofluid, Journal of Mechanical, Engineering and Science, Vol. 6, pp. 1-11. https://doi.org/10.1177%2F0954406212445683.

Alsabery, A.I., Chamkhab, A.j., salehd, H., Hashima, I., and Chananee, B.(2017): Effect of spatial side-wall temperature variations on transient natural convection of a nonofluid in a trapezoidal cavity, International Journal of Numerical Methods Heat Fluid Flow, Vol. 27, pp. 1365-1384.

Sheremet, M.A., and Pop, I. (2014): Natural convection in square porous cavity with sinusoidal temperature distributions on both side walls filled with a nanofluid: Buongiorno's model", Transport in Porous Media, Vol. 105, pp. 411-429. https://doi.org/10.1007/s11242-014-0375-7.

Sivasankaran, S., and Bhuvaneswari, M. (2013): Natural convection in porous cavity with sinusoidal heating on both sidewalls, Numerical Heat Transfer Part A: Applications, Vol. 63, pp. 14-30. https://doi.org/10.1080/10407782.2012.715985.

Priam S.S., and Nasrin, R. (2021): Oriented magneto-conjugate heat transfer and entropy generation in an inclined domain having wavy partition", International Communication in Heat and Mass Transfer, Vol. 126, 105430. https://doi.org/10.1016/j.icheatmasstransfer.2021.105430.

Malvandi, A., Heysiattalab, S., and Ganji, D.D. (2016): Thermophoresis and Brownian motion effect on heat transfer enhancement at film boiling of nanofluids over a vertical cylinder, Journal of Molecular Liquids, Vol. 216, pp. 503-509. https://doi.org/10.1016/j.molliq.2016.01.030.

Garoosi, F., Jahanshaloo, L., Rashidi, M.M., Badakhsh, A., and Ali, M.E. (2015): Numerical simulation of natural convection of the nanofluid in heat exchangers using a Buongiorno model, Applied Mathematics and Computation, Vol. 254, pp. 183-203. https://doi.org/10.1016/j.amc.2014.12.116.

Garoosi, F., Garoosi, S., and Hooman, K. (2014): Numerical simulation of natural convection and mixed convection of the nanofluid in a square cavity using Buongiorno model, Powder Technology, Vol. 268, pp. 268-292. https://doi.org/10.1016/j.powtec.2014.08.006.

Sayyar, R. O., and Saghafian, M. (2017): Numerical simulation of convective heat transfer of nonhomogeneous nanofluid using Buongiorno's model, Heat and Mass Transfer, Vol. 53, pp. 2627-2636. https://doi.org/10.1007/s00231-017-2008-5.

Malvandi, A., and Ganji, D.D. (2014): Brownian motion and thermophoresis effects on slip flow of alumina water nanofluid inside a circular microchannel in the presence of a magnetic field, International Journal of Thermal Sciences, Vol. 84, pp. 196-206. https://doi.org/10.1016/j.ijthermalsci.2014.05.013.

Kata, S., Ganganapall, S., and Kuppalapalle, V. (2019): Effect of thermophoresis and Brownian motion on the melting heat transfer of a Jeffrey fluid near a stagnation point towards a stretching surface: Buongiorno's model, Heat Transfer, Vol. 48, pp. 3328-3349. https://onlinelibrary.wiley.com/toc/15231496/2019/48/7.

Qasim, M., Khan, Z.H., Lopez, R.J., and Khan, W.A. (2016): Heat and mass transfer in a nanofluid thin film over an unsteady stretching sheet using Buongiorno's model, The European Physical Journal Plus, Vol. 131, 16. https://doi.org/10.1140/epjp/i2016-16016-8.

Pop, I., Ghalambaz, M., and Sheremet, M., (2016): Free convection in a square porous cavity filled with a nanofluid using thermal non-equilibrium and Buongiorno models, *International Journal of Numerical Methods for Heat and Fluid Flow,* Vol. *26*, pp. 671-693. https://doi.org/10.1108/HFF-04-2015-0133.

Zargartalebi, H., Ghalambaz, M., Noghrehabadi, A. Chamkha, A.J. (2016): Natural convection of a nanofluid in an enclosure with an inclined local thermal non-equilibrium porous fin considering Buongiorno's model, International Journal of Computation and Methodology, Vol. 70, pp. 432-445. https://doi.org/10.1080/10407782.2016.1173483.

Noghrehabadi, A., Behseresht, A., and Ghalambaz, M. (2013): Natural convection of nanofluid over vertical plate embedded in a porous medium: Prescribed surface heat flux, Applied Mathematics and Mechanics, Vol. 34, pp. 669-686. https://doi.org/10.1007/s10483-013-1699-6.

Sayyar, R.O., and Saghafian, M. (2017): Numerical simulation of convective heat transfer of nonhomogeneous nanofluid using Buongiorno model, Heat and Mass transfer, Vol 53, pp. 2627–2636. https://doi.org/10.1007/s00231-017-2008-5

Ali, M., Nasrin, R., and Alim, M.A. (2021): Analysis of boundary layer nanofluid flow over a stretching permeable wedge-shaped surface with magnetic effect, Journal of Naval Architecture and Marine Engineering, Vol. 18(1), 11-24. http://dx.doi.org/10.3329/jname.v18i1.44458.

Soleimani, S. Sheikholeslami, M. Ganji, D.D., and Gorji-Bandpay, M. (2012): Natural convection heat transfer in a nanofluid filled semi-annulus enclosure, *International Communications* in *Heat* and *Mass Transfer,* Vol. 39(4), pp. 565-574. https://doi.org/10.1016/j.icheatmasstransfer.2012.01.016.

Sheremet. M.A, Groşan, T., and Pop, I. (2015): Steady-state free convection in a right-angle porous trapezoidal cavity filled by a nanofluid: Buongiorno's mathematical model, *European* Journal of Mechanics-*B/Fluids,* Vol. 53, pp. 241-250. https://doi.org/10.1016/j.euromechflu.2015.06.003.

Garoosi, F., Jahanshaloo, L., Rashidi, M.M., Badakhsh, A., and Ali, M.E. (2015): Numerical simulation of natural convection of the nanofluid in heat exchangers using a Buongiorno model, Applied Mathematics and Computation, Vol. 254, pp. 183-203. https://doi.org/10.1016/j.amc.2014.12.116.

Al-Weheibi, S.M., Rahman, M.M. Alam, M.S., and Vajravelu, K. (2017): Numerical simulation of natural convection heat transfer in a trapezoidal enclosure filled with nanoparticles, International Journal of Mechanical Science, Vol. 131, pp. 599-612, 2017. https://doi.org/10.1016/j.ijmecsci.2017.

Esfe, M.H., Arani, A.A.A., Yan, W.M., Ehteram, H., Aghaie, A., and Afrand, M. (2016): Natural convection in a trapezoidal enclosure filled with carbon nanotube–EG–water nanofluid, International Journal of Heat and Mass Transfer, Vol. 92, pp. 76-82. http://dx.doi.org/10.1016/j.ijheatmasstransfer.2015.08.036.

Nasrin R., and Hossain M.S. (2021): Numerical analysis of photovoltaic power generation in different locations of Bangladesh, Journal of Computational and Applied Research in Mechanical Engineering, Vol. 10(2), pp. 373-389. https://doi.org/10.22061/JCARME.2019.4601.1558.

Ramachandra, R.V., and Suryanarayana, R.M. (2018): Heat and Mass transfer analysis of Buongiorno's model nanofluid over a linear and nonlinear stretching surface with thermal radiation and chemical reaction, Research Journal of Pharmacy and Technology, Vol. 11, pp. 4527-4533. DOI: 10.5958/0974-360X.2018.00828.4.

Khan, J.A., Mustafa, M., Hayat, T., Turkyilmazoglu, M., and Alsaedi, A. (2017) Numerical study of nanofluid flow and heat transfer over a rotating disk using Buongiorno's model, International Journal of Numerical Methods for Heat and Fluid Flow, Vol. 27, pp. 221-234. https://doi.org/10.1108/HFF-08-2015-0328.

Demirdzic, I., Lilek, Z., and Peric, M., (1992): Fluid flow and heat transfer test problems solutions for non-orthogonal grids: Benchmark, International Journal of Numerical Methods in Fluids, Vol. 15, pp. 329–354. https://doi.org/10.1002/fld.1650150306.

De Davis, G., Jones, I.P. (1983): Natural convection in a square cavity: A benchmark numerical solution, International Journal of Numerical Methods in Fluids, Vol. 3, pp. 227–248. https://doi.org/10.1002/fld.1650030304.

Venkatadri, K. Gaffar, SA., Prasad, VR., Khan, BHM., Beg, OA. (2019): Simulation of natural convection heat transfer in a 2-D trapezoidal enclosure, International Journal of Automotive and Mechanical Engineering, Vol. 16, pp. 7375-7390. http://usir.salford.ac.uk/id/eprint/56152.

Ali, M., Alim, M.A., Nasrin, R., Alam, M.S., Munshi, M.J.H. (2017): Similarity solution of unsteady MHD boundary layer flow and heat transfer past a moving wedge in a nanofluid using the Buongiorno model, Procedia Engineering, Vol. 194(C), pp. 407-413. https://doi.org/ 10.1016/j.proeng.2017.08.164.

Rahman, M.S., Nasrin, R., Hoque, M.I. (2018): Heat-mass transfer of a nanofluid in a lid-driven enclosure under three convective modes, GANIT Journal, Vol. 38, pp. 73-83. https://doi.org/10.3329/ganit.v38i0.39787.

Nasrin, R., Alim, M.A, Ali, Chamkha, J. (2013): Effect of heating wall position on forced convection along with two-sided open enclosure with porous medium utilizing nanofluid", International Journal of Energy & Technology, Vol. 5(9), pp. 1-13. https://www.academia.edu/33374983.

Ishrat Zahan, Nasrin, R., and Alim, M.A. (2018): MHD effect on conjugate heat transfer in a nanofluid filled rectangular enclosure, International Journal of Petrochemical Science and Engineering, Vol. 3, pp. 114-123. https://doi.org/10.15406/ipcse.2018.03.00085.

Nasrin, R., Hossain, S., Zahan, I., Ahmed, K.F.U. and Fayaz, H. (2020): Performance analysis of hybrid nanofluid on the enhancement of fluid thermal conductivity in lid-driven undulated cavity, Heat Transfer, 49(8), 4204 – 4225, https://doi.org/10.1002/htj.21823.

Taylor, C., Hood, P. (1973): A numerical solution of the Navier-Stokes's equations using finite element technique, Computer and Fluids, Vol. 1, pp. 73–100. https://doi.org/10.1016/0045-7930(73)90027-3.

Nasrin, R., Sweety S.A. and Zahan, I. (2021): Turbulent nanofluid flow analysis passing a shell and tube thermal exchanger with Kays-Crawford model, Journal of Nanofluids, Vol. 10, No. 4, pp. 536-555. https://doi.org/10.1166/jon.2021.1803.

Buongiorno, J. (2006): Convective transport in nanofluids, ASME Journal of Heat Transfer, Vol. 128, pp. 240-250. https://doi.org/10.1115/1.2150834